Indonesian Journal of Electrical Engineering and Computer Science
Vol. 42, No. 3, June 2026, pp. 699∼707
ISSN: 2502-4752, DOI: 10.11591/ijeecs.v42.i3.pp699-707

Parameter identification and continuous friction modelling of a brushed DC motor

Ahmad 'Abdan Syakuro[1], Vani Virdyawan[1], Sri Raharno[1], Indrawanto[1], Tegoeh Tjahjowidodo[2]
[1]Engineering Design and Production Research Group, Faculty of Mechanical and Aerospace Engineering - Institut Teknologi Bandung, Bandung, Indonesia
[2]Department of Mechanical Engineering, KU Leuven, Jan Pieter de Nayerlaan 5, Sint-Katelijne-Waver, Belgium

Article Info

Article history:

Received Aug 5, 2025
Revised Apr 8, 2026
Accepted May 26, 2026

Keywords:

Control system design
DC motor
Dynamic modelling
Friction modelling
Parameter identification

ABSTRACT

Designing high-performance control systems for brushed DC motors is often hindered by the lack of comprehensive dynamic parameters in manufacturer datasheets, particularly for low-cost DC motors. In addition to the parameter identification method, this study also introduces a continuously differentiable friction model incorporating Coulomb and viscous-like behaviors using a hyperbolic tangent function. The electrical and mechanical parameters of an RS-775 motor were identified using standard laboratory tools and the MATLAB system identification toolbox. The proposed model was validated against experimental data under square wave and sinusoidal inputs, achieving a position prediction error of less than 5% and capturing complex dynamic behaviors. The results demonstrate that this accessible identification approach provides a sufficiently accurate dynamic model for educational and industrial robotics applications, offering a superior alternative to trial-and-error tuning.

Corresponding Author:

Vani Virdyawan
Engineering Design and Production Research Group
Faculty of Mechanical and Aerospace Engineering - Institut Teknologi Bandung
40132 Coblong, Bandung, Indonesia
Email: vani.virdyawan@itb.ac.id

1. INTRODUCTION

In industrial automation and robotics, the brushed DC motor remains an ubiquitous actuator due to its simplicity and cost-effectiveness [1]. However, achieving precise trajectory tracking requires an accurate mathematical model. Although classical strategies like proportional-integral-derivative (PID) can be tuned heuristically, this trial-and-error approach is inefficient and often fails to meet strict performance requirements [2]-[4]. Trial-and-error tuning methods are often time-consuming and effort-intensive [5], which can be problematic when addressing complex control requirements or when striving for optimal performance. To overcome these limitations and fulfill more intricate requirements, such as precise trajectory tracking and robust disturbance rejection, accurate mathematical models of the system are essential.

A significant challenge for control engineers is that low-cost motor datasheets typically provide only static parameters (e.g., stall torque), omitting critical dynamic terms such as rotor inertia and non-linear friction coefficients [6]. Furthermore, physical wear can cause these parameters to drift over time, making the datasheet values obsolete [7], [8].

To address this, several system-identification methods can be used, including the inverse-problem approach [9], the algebraic identification method [7], modified least squares methods [10], [11], and optimiza-

tion methods [12], [13]. Recent literature has explored advanced techniques, including genetic algorithms [14] and data-driven black-box modeling [15]. Although effective, these methods often require high computational power or lose the physical meaning of the parameters. Other techniques rely on expensive torque sensors or coupled generator setups [16], which may not be accessible for low-cost projects [17].

This paper addresses this gap by presenting a practical, sensor-minimalist methodology. The primary contribution is the integration of a continuously differentiable friction model (using a hyperbolic tangent function). This approach captures non-linear friction effects critical for low-speed control [18] without introducing the computational discontinuities found in classical Coulomb models [19]. Furthermore, unlike the linear friction model [8], [20] that does not use Coulomb friction, this work incorporates Coulomb friction to improve current control accuracy, as poor current prediction occurs when only viscous friction is used.

2. METHOD

2.1. DC motor model

The armature circuit of a DC motor can be represented by a series of resistance (R_a) and an inductance (L_a). Given the standard armature R–L model, we omit the schematic for brevity. When a voltage (V_{in}) is applied across the motor terminals, it drives a current (I_a) through the armature winding. This current interacts with the magnetic field produced by the stator (typically by permanent magnets) to generate a torque (T) on the rotor. According to Lenz's law, as the rotor spins within this magnetic field, it induces a back electromotive (back-EMF) voltage (V_e) that opposes the applied voltage, which is represented in (1). The generated electromagnetic torque (T) is directly proportional to the armature current as $T = K_t I_a$, where K_t is the torque constant of the motor. Similarly, the back-EMF voltage is directly proportional to the angular velocity (ω) [11] of the rotor as $V_e = K_b\omega$, where K_b is the back-EMF constant.

The rotor of the DC motor is the mechanical part that rotates, driven by the electromagnetic torque. Its motion follows Newton's second law for rotational systems, which states that the net torque acting on the rotor is equal to the product of its moment of inertia (J) and its angular acceleration. In a geared motor, the effective rotor inertia is increased by a factor of N^2 due to the load inertia (J_L). The torques acting on the rotor typically include the electromagnetic torque and the friction torque (T_f) as shown in (2). In this parameter identification process, the motor is operated without an external mechanical load coupled to the gearbox output shaft. Therefore, we assume the external load torque $T_{load} \approx 0$, and the reflected load inertia J_L consists only of the gearbox internal components.

$$L_a \frac{\mathrm{d}I_a}{\mathrm{d}t} + R_a I_a = V_{in} - V_e \tag{1}$$

$$J\frac{\mathrm{d}\omega}{\mathrm{d}t} = (J_m + \frac{J_L}{N^2})\frac{\mathrm{d}\omega}{\mathrm{d}t} = T - T_f - \frac{T_{load}}{N} \tag{2}$$

Friction in DC motors is a complex phenomenon that significantly affects the motor's performance, especially at low speeds. Friction in the classical model of a DC motor only consists of viscous friction, but the general friction can be expressed as a combination of three main components: Stribeck friction, Coulomb friction, and viscous friction [21]. One of the classical friction models can be represented as in (3). Where T_f is the total friction torque, T_s represents the Stiction (also known as static friction) that has Stribeck effect effective until the Stribeck velocity (ω_s), T_c is the Coulomb friction, and B is the viscous friction coefficient.

More advanced friction models have been developed to capture the behaviors observed in real systems. These include Dahl model [22], LuGre model [23], and generalized maxwell slip (GMS) [24], [25]. As these models are discontinuous or piecewise continuous, this could cause a problem in the control application. Therefore, in applications, it is favorable to use a continuously differentiable friction model [26] as in (4).

$$T_f = (T_s - T_c)e^{-(\frac{\omega}{\omega_s})^2} + T_c\text{sign}(\omega) + B\omega \tag{3}$$

$$T_f = \alpha_1 \tanh(\beta_1\omega) - \tanh(\beta_2\omega) + \alpha_2 \tanh(\beta_3\omega) + \alpha_3\omega \tag{4}$$

The choice of friction model depends on the requirements, the desired accuracy of the motor model, and the resources available. For simpler applications or initial modeling stages, the linear viscous friction often offers an ease in simulation.

2.2. DC motor parameter identification

The parameter identification process use an experimental setup and follows a series of steps summarized in Figure 1. The armature resistance and inductance of the DC motor were determined by direct measurement. The armature resistance was measured by recording the resistance between two motor terminals using an Ohmmeter (Model CD800a, Sanwa Electric Instrument Co., Ltd., Tokyo, Japan). The armature inductance was measured by recording the inductance between two motor terminals using an LCR meter (Model LCR700, Sanwa Electric Instrument Co., Ltd., Tokyo, Japan).

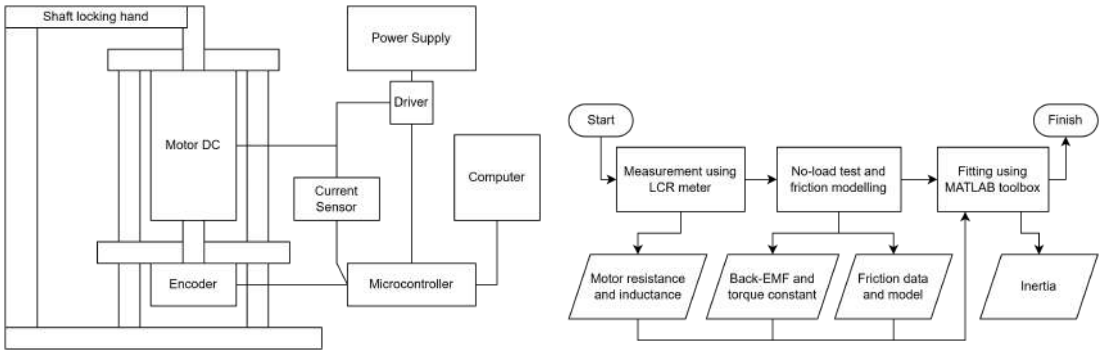

Figure 1. Experimental setup (left) and steps for motor parameter identification (right)

The back-EMF constant was determined using a no-load test. The DC motor was connected to a DC power supply (Model GPD-3303S, Good Will Instrument Co., Ltd., New Taipei City, Taiwan) and run without any external mechanical load. The applied voltage and the applied current were recorded from the power supply's display. The angular velocity of the motor shaft was measured using a rotary incremental encoder with 360 PPR (pulses per revolution). As the motor is connected to a planetary gearhead (ratio 19.2:1), the effective resolution of the encoder is 0.052° (equal to 6912 PPR). The back-EMF was calculated by accounting for the voltage drop across the armature resistance using Kirchhoff's voltage law. The back-EMF constant was then calculated using the relationship shown in (5).

$$K_b = \frac{V_e}{\omega} = \frac{V_{in} - I_a R_a}{\omega} \tag{5}$$

Where ω is the no-load steady-state angular velocity in radians per second. The torque constant (K_t) of the DC motor was assumed to be approximately equal to the back-EMF constant ($K_t \approx K_b$). This assumption is based on the theoretical principle that for an ideal DC motor in SI units, these two constants have the similar numerical value when there is little to no energy losses.

The friction model was estimated by analyzing the steady-state torque-velocity relationship obtained from the same no-load tests conducted to determine the back-EMF constant. The torque acting on the rotor was calculated using $T = K_t I_a$. This torque must overcome the frictional torques at steady-state under no external load. To reduce the complexity but still maintain accurate friction modeling, the total friction torque was modeled as a combination of viscous friction (proportional to velocity) and Coulomb friction (a constant opposing motion), represented by (6). Classical Coulomb models use a discontinuous 'sign' function, which causes numerical chattering. To resolve this, we approximate friction using a continuous hyperbolic tangent function [26], represented by (7), where β determines the steepness of the transition. This ensures numerical stability during parameter identification [19].

$$T_f = T_c \text{sign}(\omega) + B\omega \tag{6}$$

$$T_f = T_C \tanh(\beta\omega) + B\omega \tag{7}$$

The values of the viscous friction coefficient and Coulomb friction (T_c) were estimated by plotting the calculated torque against the measured steady-state angular velocity for different applied voltages (and thus different operating speeds). Due to the coupled friction components, the overall friction model was identified

altogether using the least-square technique. This involved linear regression of the friction at non-near-zero speed ranges to get the slope of viscous friction. The speed range used is from 5 rad/s to the maximum speed of 58 rad/s, to avoid the Stribeck effect at near-zero speed. The minimum friction at a non-zero speed was used to determine the coulomb friction. As we observed the asymmetricity of friction at different rotation direction, we use the average value of B and T_c from the clockwise and counterclockwise tests. The result of this method can be seen at Figure 2, with $B = 0.0012\ \frac{\text{Nm}}{\text{rad/s}}$ and $T_c = 0.140$ Nm. The Stribeck effect, which describes the non-linear friction behavior at very low speeds, was observed in the experimental data but was assumed to be negligible for the simplicity of the model. Using this method, the RMS error of the friction force (at non-zero speed) is 0.02 Nm which shows that this model has the potential to predict the actual friction.

The motor inertia (J) was estimated by analyzing the transient speed response of the motor to step voltage inputs of varying magnitudes under no-load conditions. As a sudden rise in voltage induces in-rush current, the current needed to generate a step-shaped voltage is relatively high. The same experimental setup used for the back-EMF constant determination was utilized. The power supply used has a maximum current of 6.4 A (in parallel mode), which limits the magnitude of step voltage that can be generated up to around 9 V. To ensure the steepness of the step voltage, the tests will vary the magnitude of the step voltage to be 2, 4, 6, and 8 V.

The experimental speed response data, along with the calculated input torque (8), were then analyzed using the system identification toolbox in MATLAB (MathWorks, Natick, MA, USA). A first-order transfer function model relating the input torque to the angular velocity, as in (9), was fitted to the experimental data. The toolbox estimated the gain (K) and pole (p) of this first-order system. The inertia was then calculated from the gain using the relationship $J = 1/K$, resulting in $J = 0.0031 \pm 0.0003\ \text{kgm}^2$. While the pole $p = B/J$ could be used to estimate the viscous friction coefficient, we need to note that the tests were only performed with step input below 9 V (equivalent to a steady-state velocity of 20 rad/s), which does not represent all of the friction profile as seen in Figure 2. The viscous coefficient determined with this method has a value of $B = 0.0033 \pm 0.0024\ \frac{\text{Nm}}{\text{rad/s}}$, which is much higher than the viscous coefficient from the regression of the steady-state response method $B = 0.0012\ \frac{\text{Nm}}{\text{rad/s}}$. As the regression method uses data from all velocity range (except near-zero velocity), it is more logical to use the regression of the steady-state response method to determine the viscous coefficient for general use.

$$T_{in} = K_t I - T_c \text{sign}(\omega) \tag{8}$$

$$\frac{\omega(s)}{T_{in}(s)} = \frac{1}{Js + B} \tag{9}$$

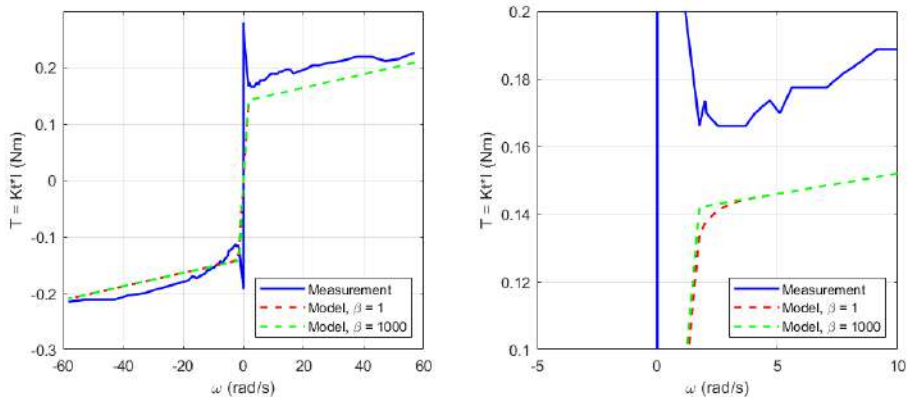

Figure 2. Friction model using coulomb and viscous friction components (left) and the effect of different β value (right). The higher β increases the similarity of the model to viscous friction phenomenon while the lower β reduce the steepness of the model, especially around zero-velocity, which increase the numerical stability

2.3. Model performance testing

The experimental setup for model validation consisted of the following components: the characterized DC motor RS-775, a DC power supply, an IBT-2 motor driver module based on the BTS7960 high-current half-bridge (Infineon Technologies AG, Munich, Germany), an ESP32 microcontroller (Espressif Systems, Shanghai, China) for PWM generation and data acquisition, a current sensor for current measurement, and an incremental encoder with 360 PPR for angular position measurement. The encoder readings were captured using an interrupt routine on the ESP32 to ensure accurate position measurements, while the other measurements were acquired by sampling time of 1 ms. Two types of input voltage signals were used to test the model's performance across different operating regimes:

a. Square wave input: square wave voltage signals with a period of 4 seconds (2 seconds at a constant high voltage, followed by 2 seconds at 0 V) were applied. Three different high voltage levels were tested: 3, 6, and 9 V. Each test began with the input voltage at 0 V.
b. Sinusoidal input: sinusoidal voltage signals with a period of 4 seconds were applied, starting at 0 V. The crest amplitudes of the sine waves were set to 3, 6, and 9 V, with the trough at 0 V.

The identified DC motor model was simulated in MATLAB for 12 seconds with a fixed-step solver and a sampling period of $T = 10^{-4}$ seconds (10 kHz) to ensure numerical stability. The difference equations in (10)-(12) were derived from the differential equation of the DC motor dynamic model, by applying the backward difference approximation for the derivative. These difference equations were used for the simulation. In (10)-(12), I is the armature current, ω is the angular velocity, θ is the angular position, and V_{in} is the input voltage. The motor parameters R_a, L_a, K_b, K_t, B, T_c, and J used in the simulation were the values identified through the procedures described in section 3.1. The value of β was determined heuristically by observing the instability at zero velocity, with the obtained value of $\beta = 214$. To benchmark the proposed model's performance, a comparison is conducted against a classic linear model where Coulomb friction is neglected ($T_c = 0$). To ensure a fair comparison, the viscous friction coefficient for this linear model was recalculated via linear regression across the full velocity range (-58 to 57 rad/s), yielding $B = 0.0064 \frac{\text{Nm}}{\text{rad/s}}$.

$$I(k) = I(k-1) + \frac{V_{in}(k-1) - R_a I(k-1) - K_b \omega(k-1)}{L_a} T \tag{10}$$

$$\omega(k) = \omega(k-1) + \frac{K_t I(k-1) - B\omega(k-1) - T_c \tanh(\beta\omega(k-1))}{J} T \tag{11}$$

$$\theta(k) = \theta(k-1) + \omega(k-1)T \tag{12}$$

3. RESULTS AND DISCUSSION

For the square wave voltage inputs, the comparison between the simulated and experimental armature current, as shown in the first column of Figure 3, revealed that the model generally predicted the rising and falling peaks of the current with reasonable accuracy. However, an overshoot error was observed, where the simulated current overshoot deviated from the overshoot current measured experimentally. The test with 9 V square wave input has an average overshoot error of 33% and average undershoot error of 31%. This discrepancy suggests a potential difference in the actual effective resistance of the motor windings under operation compared to the static resistance value used in the model, likely due to heating. The comparison of the angular velocity profiles for the tests with square wave input showed that while the model captured the general trend of the motor's acceleration and deceleration, the rise time to the steady-state speed in the simulation sometimes differed slightly from the experimental data, possibly due to minor inaccuracies in the identified inertia or friction parameters. The steady-state speeds generally showed good agreement with 0.7% NRMSE for the 9V test, although the current error likely contributed to minor differences in torque generation.

For the tests with sinusoidal voltage input, the comparison of the armature current showed that the model's prediction accuracy varied throughout the sinusoidal cycle. A notable discrepancy occurred during peak angular deceleration (20.5%), where the simulated current deviated more from experimental values compared to peak acceleration (1.6%) and around peak velocity (7.7%). This suggests potential inaccuracies in the model's representation of dynamic torques during deceleration, influenced by motor inertia and friction, which are likely due to the estimation of rotor inertia and the simplified friction model. The velocity profiles

generally captured the sinusoidal trend, but a difference of 2.3% NRMSE existed on the 9V test. These discrepancies likely result from combined inaccuracies in current prediction and the limitations of the first-order mechanical model.

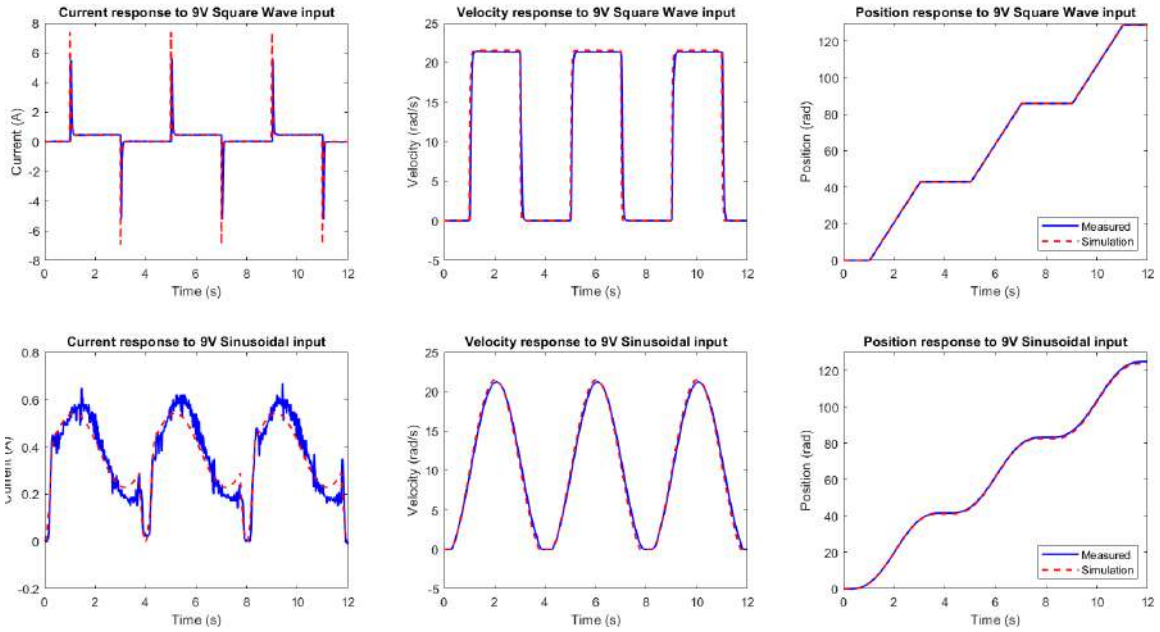

Figure 3. Comparison of measured (solid blue) and simulated (dashed red) armature current, angular velocity, and angular position when the motor is subjected to square wave an sinusoidal inputs of 9 V peak voltage

Overall, the model can predict the behavior of the DC motor. Some parameters have higher RMSE, especially in higher input voltage. Table 1 shows that the velocity in tests with square wave input has a higher RMSE at higher voltages. The RMSE increases by approximately 0.5 rad/s for each 3 V increase in input voltage. This is believed due to the properties of a DC motor: the velocity is proportional to the input voltage. Unlike the tests with square wave input, the RMSE in the sinusoidal tests does not show a clear proportionality to the input voltage. This occurs because the RMSE is calculated over the entire motion profile, where the steepness is heavily influenced by the acceleration. Interestingly, the same occurrence happens to the in-rush current from the tests with square wave input. In the initial rising of the tests with square wave input, the rotor is not rotating yet, producing near-zero back-EMF voltage and turning the relation of current and input voltage to be proportional. This relation contributes directly to the almost proportional current RMSE increase by 0.2 A for each 3 V input voltage increase.

Table 1. RMSE and NRMSE from the first 10 seconds of simulation

		Square wave inputs			Sinusoidal inputs		
	Parameter	3V	6V	9V	3V	6V	9V
Root mean	Current (A)	0.21	0.41	0.62	0.07	0.05	0.05
Square error	Velocity (rad/s)	0.51	1.00	1.58	0.31	0.33	0.48
(RSME)	Position (rad)	0.82	0.24	0.09	1.48	0.85	0.48
Normalized	Current	5.9%	5.7%	5.7%	11.1%	8.7%	7.6%
RMSE	Velocity	7.5%	7.1%	7.3%	4.6%	2.4%	2.3%
(NRMSE)	Position	2.4%	0.3%	0.1%	4.8%	1.3%	0.5%
NRMSE,	Current	7.3%	5.9%	5.8%	37.3%	35.4%	29.5%
without T_C,	Velocity	9.1%	7.5%	7.4%	8.5%	4.7%	3.4%
$B = 0.0064\frac{Nm}{rad/s}$	Position	4.4%	1.8%	0.7%	9.1%	4.4%	2.6%

The 11.1% current NRMSE with sinusoidal inputs was caused by the friction model's inaccuracy, particularly at low speeds where the unmodeled Stribeck effect is most influential. A consistent finding was

lower prediction NRMSE at higher input voltages (9V), with the lowest NRMSE of 0.1%, likely due to the simplified friction model neglecting the Stribeck effect and continuous Coulomb friction at very low speeds. The overshoot current error for tests with square wave input suggests a need for refinement of electrical parameters like armature resistance and the back-EMF constant, possibly considering temperature dependency. Dynamic errors in sinusoidal tests point to potential inaccuracies in mechanical parameters (rotor inertia and friction), suggesting the need for more complex models or identification techniques. Despite these limitations, the developed model provides a better representation of the motor's dynamics compared to the classic linear model. To provide a fair comparison with the classic linear model, which omits Coulomb friction, the viscous damping coefficient was recalculated using linear regression across the entire friction profile, resulting in $B = 0.0064 \frac{\text{Nm}}{\text{rad/s}}$. The absence of Coulomb friction resulted in a relatively poor current prediction, with 37.3% NRMSE, compared to the 11.1% NRMSE in the proposed model.

4. CONCLUSION

This study successfully bridges the gap of limited information on low-cost motor datasheets parameters by proposing a methodology used to identify various motor parameters. Specifically for the mechanical subsystem, a friction model based on a continuously differentiable hyperbolic tangent function is proposed, which demonstrates current, velocity, and position NRMSE below 7.5% in capturing the motor's behavior under rapid change in input voltage. Unlike standard Coulomb approaches, this method eliminates numerical chattering, enabling efficient parameter estimation using standard laboratory tools. Experimental validation confirmed that the model achieves high accuracy in position tracking with NRMSE below 5%, establishing it as a superior alternative to classic linear model. While dynamic tracking at low speeds exhibits deviations due to the simplification of Stribeck effects, the model captures the essential non-linearities required to model the motor. Future work will focus on integrating thermal dynamics and adaptive friction compensation to explicitly address these low-speed tracking performance.

FUNDING INFORMATION

This work is funded by Research and Community Service Program (PPMI) 2025, Faculty of Mechanical and Aerospace Engineering, Institut Teknologi Bandung.

AUTHOR CONTRIBUTIONS STATEMENT

This journal uses the Contributor Roles Taxonomy (CRediT) to recognize individual author contributions, reduce authorship disputes, and facilitate collaboration.

Name of Author	C	M	So	Va	Fo	I	R	D	O	E	Vi	Su	P	Fu
Ahmad 'Abdan Syakuro	✓	✓	✓	✓	✓	✓	✓	✓	✓	✓	✓			
Vani Virdyawan		✓				✓	✓			✓		✓	✓	✓
Sri Raharno						✓				✓		✓	✓	
Indrawanto						✓				✓		✓	✓	
Tegoeh Tjahjowidodo						✓				✓		✓	✓	

C : **C**onceptualization
M : **M**ethodology
So : **So**ftware
Va : **Va**lidation
Fo : **Fo**rmal Analysis
I : **I**nvestigation
R : **R**esources
D : **D**ata Curation
O : Writing - **O**riginal Draft
E : Writing - Review & **E**diting
Vi : **Vi**sualization
Su : **Su**pervision
P : **P**roject Administration
Fu : **Fu**nding Acquisition

CONFLICT OF INTEREST STATEMENT

There is no conflict of interest in the process of writing this paper.

DATA AVAILABILITY

Derived data supporting the findings of this study are available from the corresponding author, Vani Virdyawan, on request.

REFERENCES

[1] Z. Ali *et al.*, "Design and development of a low-cost 5-DOF robotic arm for lightweight material handling and sorting applications: a case study for small manufacturing industries of Pakistan," *Results in Engineering*, vol. 19, p. 101315, Sep. 2023, doi: 10.1016/j.rineng.2023.101315.

[2] M. Khalifa, A. H. Amhedb, and M. Al Sharqawi, "Position control of real time DC motor using LabVIEW," *Journal of Robotics and Control (JRC)*, vol. 2, no. 5, pp. 391–397, 2021, doi: 10.18196/jrc.25104.

[3] M. S. Chehadeh and I. Boiko, "Design of rules for in-flight non-parametric tuning of PID controllers for unmanned aerial vehicles," *Journal of the Franklin Institute*, vol. 356, no. 1, pp. 474–491, Jan. 2019, doi: 10.1016/j.jfranklin.2018.10.015.

[4] O. Janos and P. Dobra, "H_∞ controller design and parametric identification for a DC brushed motor," in *2022 23rd IEEE International Conference on Automation, Quality and Testing, Robotics - THETA, AQTR 2022 - Proceedings*, IEEE, May 2022, pp. 1–6, doi: 10.1109/AQTR55203.2022.9801991.

[5] P. Mitra, C. Dey, and R. K. Mudi, "Fuzzy rule-based set point weighting for fuzzy PID controller," *SN Applied Sciences*, vol. 3, no. 6, p. 651, Jun. 2021, doi: 10.1007/s42452-021-04626-0.

[6] M. D. Cook, J. L. Bonniwell, L. A. Rodriguez, D. W. Williams, and J. Pribbernow, "Low-cost DC motor system for teaching automatic controls," in *Proceedings of the American Control Conference*, IEEE, Jul. 2020, pp. 4283–4288, doi: 10.23919/ACC45564.2020.9147781.

[7] J. Becedas, G. Mamani, and V. Feliu, "Algebraic parameters identification of DC motors: methodology and analysis," *International Journal of Systems Science*, vol. 41, no. 10, pp. 1241–1255, Oct. 2010, doi: 10.1080/00207720903244097.

[8] S. S. Saab and R. A. Kaed-Bey, "Parameter identification of a DC motor: an experimental approach," in *ICECS 2001. 8th IEEE International Conference on Electronics, Circuits and Systems (Cat. No.01EX483)*, IEEE, 2001, pp. 981–984, doi: 10.1109/ICECS.2001.957638.

[9] M. Hadef and M. R. Mekideche, "Parameter identification of a separately excited dc motor via inverse problem methodology," *Turkish Journal of Electrical Engineering and Computer Sciences*, vol. 17, no. 2, pp. 99–106, Jan. 2009, doi: 10.3906/elk-0805-5.

[10] R. Krneta, S. Antic, and D. Stojanovic, "Recursive least squares method in parameters identification of DC motors models," *Facta universitatis - series: Electronics and Energetics*, vol. 18, no. 3, pp. 467–478, 2005, doi: 10.2298/fuee0503467k.

[11] M. Li and Y. Ma, "Parameter identification of DC motor based on compound least square method," in *Proceedings of 2020 IEEE 5th Information Technology and Mechatronics Engineering Conference, ITOEC 2020*, IEEE, Jun. 2020, pp. 1107–1111, doi: 10.1109/ITOEC49072.2020.9141652.

[12] S. Adewusi and T. Tomasetti, "Modeling and parameter identification of a DC motor using constraint optimization technique," *IOSR Journal of Mechanical and Civil Engineering (IOSR-JMCE) e-ISSN*, vol. 13, no. 6, pp. 46–56, 2016, [Online]. Available: www.iosrjournals.org.

[13] B. Nayak and S. Sahu, "Parameter estimation of DC motor through whale optimization algorithm," *International Journal of Power Electronics and Drive Systems (IJPEDS)*, vol. 10, no. 1, pp. 83–92, Mar. 2019, doi: 10.11591/ijpeds.v10.i1.pp83-92.

[14] M. S. Amiri, M. F. Ibrahim, and R. Ramli, "Optimal parameter estimation for a DC motor using genetic algorithm," *International Journal of Power Electronics and Drive Systems (IJPEDS)*, vol. 11, no. 2, pp. 1047–1054, Jun. 2020, doi: 10.11591/ijpeds.v11.i2.pp1047-1054.

[15] M. A. Khan, D. E. Ze. Baig, H. Ali, and F. R. Albogamy, "Optimized system identification (SI) of Brushless DC (BLDC) motor using data-driven modeling methods," *Scientific Reports*, vol. 15, no. 1, p. 8497, Mar. 2025, doi: 10.1038/s41598-025-93444-0.

[16] M. L. Hamida, A. Fekik, H. Denoun, and F. Kadi, "Experimental identification and control of a 3Kw DC motor," *Periodica polytechnica Electrical engineering and computer science*, vol. 66, no. 4, pp. 301–314, Oct. 2022, doi: 10.3311/PPee.20421.

[17] M. F. Fazdi and P. W. Hsueh, "Parameters identification of a permanent magnet DC motor: a review," *Electronics (Switzerland)*, vol. 12, no. 12, p. 2559, Jun. 2023, doi: 10.3390/electronics12122559.

[18] B. Li, X. Xie, B. Yu, Y. Liao, and D. Fan, "High-precision velocity control of direct-drive systems based on friction compensation," *Mechanical Sciences*, vol. 15, no. 1, pp. 385–394, Jun. 2024, doi: 10.5194/ms-15-385-2024.

[19] C. A. Perez-Gomez, J. U. Liceaga-Castro, and I. I. Siller-Alcala, "Non-linear modeling and identification of a permanent magnet DC motor," in *Proceedings - 24th International Conference on Circuits, Systems, Communications and Computers, CSCC 2020*, IEEE, Jul. 2020, pp. 189–194, doi: 10.1109/CSCC49995.2020.00041.

[20] A. A. Bature, M. Muhammad, and A. M. Abdullahi, "Parameter identification of a class of DC motor," *International Journal of Research in Engineering and Science*, vol. 1, no. 5, pp. 69–72, 2013, [Online]. Available: http://www.ijres.org/papers/v1-i5/K0156972.pdf

[21] J. Na, X. Ren, and Q. Chen, "Modeling and control of uncertain systems with friction," in *Adaptive Identification and Control of Uncertain Systems with Non-smooth Dynamics*, 2018, pp. 11–105, doi: 10.1016/C2016-0-04487-X.

[22] P. Dahl, "A solid friction model," *Aerospace Corporation El Segundo, CA*, vol. 158, p. Tech. Rep. TOR-01 58(3 107-1 8)-1, 1968, [Online]. Available: http://oai.dtic.mil/oai/oai?verb=getRecord&metadataPrefix=html&identifier=ADA041920.

[23] C. C. de Wit, P. Lischinsky, K. J. Åström, and H. Olsson, "A new model for control of systems with friction," *IEEE Transactions on Automatic Control*, vol. 40, no. 3, pp. 419–425, Mar. 1995, doi: 10.1109/9.376053.

[24] F. Al-Bender, V. Lampaert, and J. Swevers, "The generalized Maxwell-slip model: a novel model for friction simulation and compensation," *IEEE Transactions on Automatic Control*, vol. 50, no. 11, pp. 1883–1887, Nov. 2005, doi: 10.1109/TAC.2005.858676.

[25] T. Tjahjowidodo, F. Al-Bender, and H. Van Brussel, "Friction identification and compensation in a DC motor," *IFAC Proceedings Volumes (IFAC-PapersOnline)*, vol. 38, no. 1, pp. 554–559, 2005, doi: 10.3182/20050703-6-cz-1902.00093.

[26] C. Makkar, W. E. Dixon, W. G. Sawyer, and G. Hu, "A new continuously differentiable friction model for control systems design," in *Proceedings, 2005 IEEE/ASME International Conference on Advanced Intelligent Mechatronics*, IEEE, 2005, pp. 600–605, doi: 10.1109/AIM.2005.1511048.

BIOGRAPHIES OF AUTHORS

Ahmad 'Abdan Syakuro received his master's degree in Mechanical Engineering from the Faculty of Mechanical and Aerospace Engineering, Bandung Institute of Technology (ITB), Indonesia, in 2025. He obtained his Bachelor of Engineering degree from the same faculty in 2024. His research interests focus on control engineering, particularly in the design of haptic devices for medical applications such as bone drilling. He can be contacted at email: ahmadabdan510@gmail.com.

Vani Virdyawan received the B.Sc. and M.Sc. degrees in mechanical engineering from Institut Teknologi Bandung, Indonesia, in 2010 and 2011, respectively, and the Ph.D. degree in medical robotics from Imperial College London, U.K., in 2018. He is an assistant professor in Engineering Design and Production Research Group, Faculty of Mechanical and Aerospace Engineering, Institut Teknologi Bandung, Indonesia. His research interests include laser-based sensors, machine learning, soft robotics, and medical robotics. He can be contacted at email: vani.virdyawan@itb.ac.id.

Sri Raharno is an associate professor in the Design and Manufacturing Engineering Research Group at the Faculty of Mechanical and Aerospace Engineering, Institut Teknologi Bandung (ITB), Indonesia. He holds a Doctorate from ITB, specializing in production systems and manufacturing technology. His research focuses on Intelligent Manufacturing Systems and Industry 4.0 implementation. He can be contacted at email: harnos@itb.ac.id.

Indrawanto is an associate professor at the Department of Mechanical Engineering, Institut Teknologi Bandung (ITB), Indonesia. He received the B.S. degree in mechanical engineering in 1987, from ITB, the M.S. degree in mechanical engineering in 1993, and the Ph.D. degree in mechanical engineering in 1998, both are from the Catholic University of Leuven, Belgium. His research interests include robotics, additive manufacturing, computer vision and application of artificial intelligence to robotics and manufacturing. He can be contacted at email: indrawanto@itb.ac.id.

Tegoeh Tjahjowidodo is now an associate professor at the Department of Mechanical Engineering, KU Leuven, Belgium, since 2019. He received his Ph.D. degree from the same university in 2006. From 2009 until 2019 he was serving the School of Mechanical and Aerospace Engineering, NTU, Singapore as an associate professor. He is involved in some projects related to his research interests in nonlinear dynamics, modeling, identification and control, with more focus in monitoring for manufacturing. He can be contacted at email: tegoeh.tjahjowidodo@kuleuven.be.